Journal of Hepatocellular Carcinoma

Dovepress

open access to scientific and medical research

Open Access Full Text Article

ORIGINAL RESEARCH

Peritumoral Dilation Radiomics of Gadoxetate Disodium-Enhanced MRI Excellently Predicts Early Recurrence of Hepatocellular Carcinoma without Macrovascular Invasion After Hepatectomy

Huanhuan Chong[1,2]
Yuda Gong[3]
Xianpan Pan[4]
Aie Liu[4]
Lei Chen[4]
Chun Yang[1]
Mengsu Zeng[1,2,5]

[1]Department of Radiology, Zhongshan Hospital, Fudan University, Shanghai, 200032, People's Republic of China; [2]Shanghai Institute of Medical Imaging, Shanghai, 200032, People's Republic of China; [3]Department of General Surgery, Zhongshan Hospital, Fudan University, Shanghai, 200032, People's Republic of China; [4]Shanghai United Imaging Intelligence Co., Ltd, Shanghai, 200232, People's Republic of China; [5]Department of Medical Imaging, Shanghai Medical College, Fudan University, Shanghai, 200032, People's Republic of China

Correspondence: Mengsu Zeng; Chun Yang
Department of Radiology, Zhongshan Hospital, Fudan University, 180 Feng Lin Road, Shanghai, 200032, People's Republic of China
Tel +86-21-13501922963; +86-21-18702135336
Email mengsu_zeng@163.com; dryangchun@hotmail.com

Background: Whether peritumoral dilation radiomics can excellently predict early recrudescence (≤2 years) in hepatocellular carcinoma (HCC) remains unclear.

Methods: Between March 2012 and June 2018, 323 pathologically confirmed HCC patients without macrovascular invasion, who underwent liver resection and preoperative gadoxetate disodium (Gd-EOB-DTPA) MRI, were consecutively recruited into this study. Multivariate logistic regression identified independent clinicoradiologic predictors of 2-year recrudescence. Peritumoral dilation (tumor and peritumoral zones within 1cm) radiomics extracted features from 7-sequence images for modeling and achieved average but robust predictive performance through 5-fold cross validation. Independent clinicoradiologic predictors were then incorporated with the radiomics model for constructing a comprehensive nomogram. The predictive discrimination was quantified with the area under the receiver operating characteristic curve (AUC) and net reclassification improvement (NRI).

Results: With the median recurrence-free survival (RFS) reaching 60.43 months, 28.2% (91/323) and 16.4% (53/323) patients suffered from early and delay relapse, respectively. Microvascular invasion, tumor size >5 cm, alanine aminotransferase >50 U/L, γ-glutamyltransferase >60 U/L, prealbumin ≤250 mg/L, and peritumoral enhancement independently impaired 2-year RFS in the clinicoradiologic model with AUC of 0.694 (95% CI 0.628–0.760). Nevertheless, these indexes were paucity of robustness (P >0.05) when integrating with 38 most recurrence-related radiomics signatures for developing the comprehensive nomogram. The peritumoral dilation radiomics—the ultimate prediction model yielded satisfactory mean AUCs (training cohort: 0.939, 95% CI 0.908–0.973; validation cohort: 0.842, 95% CI 0.736–0.951) after 5-fold cross validation and fitted well with the actual relapse status in the calibration curve. Besides, our radiomics model obtained the best clinical net benefits, with significant improvements of NRI (35.9%-66.1%, P <0.001) versus five clinical algorithms: the clinicoradiologic model, the tumor-node-metastasis classification, the Barcelona Clinic Liver Cancer stage, the preoperative and postoperative risks of Early Recurrence After Surgery for Liver tumor.

Conclusion: Gd-EOB-DTPA MRI-based peritumoral dilation radiomics is a potential preoperative biomarker for early recurrence of HCC patients without macrovascular invasion.

Keywords: gadoxetate disodium, hepatocellular carcinoma, radiomics, magnetic resonance imaging, neoplasm recurrence

Introduction

Hepatocellular carcinoma (HCC) is the sixth most prevalent malignancy and the third leading cause of cancer-related death globally.[1] Given that the 5-year recurrence rate after liver resection reaches 50%-70%,[2] the major obstacle to improving long-term survival is postoperative recrudescence.[3] More than 80% of relapse originates from the remnant liver, on the contexts of de novo multicentric occurrence or intrahepatic metastasis from the initial HCC.[4] The latter recurrent mechanism correlates with worse outcome, and usually manifests as early relapse (≤2 years)[5] which significantly shortens survival versus late recurrence (>2 years) after curative surgery.[3] Hence, early surveillance is key to improving prognosis.

Being the contraindication for liver resection and transplantation, macrovascular invasion (MaVI) frequently seen in the portal vein is extremely detrimental to prognosis and can be specifically distinguished by contrast-enhanced MRI.[6] As a hepatobiliary-specific contrast agent, gadoxetate disodium (Gd-EOB-DTPA; Primovist ™, Bayer Pharma AG, Berlin, Germany) can evaluate hemodynamics, hepatobiliary absorption and excretion function of the lesion[7] and identify MaVI in one-stop MRI. Contrasted to CT or MRI without hepatobiliary agent, Gd-EOB-DTPA MRI is adept in detecting early/small/additional HCC lesions, increasing accuracy for HCC diagnosis and staging, and decreasing relapse and overall mortality.[8–13] Notwithstanding Gd-EOB-DTPA MRI exerts crucial impacts on HCC management, it provides limited quantitative hallmarks than multiparameter radiomics.[14]

Radiomics, a novel and non-invasive imaging tool, can extract high-throughput and high-dimensional signatures from multi-modality imaging.[15] Draw support from machine learning algorithms, radiomics can construct clinical target-oriented imaging biomarkers to increase diagnostic or prognostic accuracy, benefit the characterization of lesions, and heighten the surveillance management of patients.[14,16] Pathologically, peritumoral parenchyma is representative of cancerous heterogeneity, rich in highly invasive cells, vulnerable to microvascular invasive (MVI) and satellite nodules, thereby promoting the occurrence of MaVI and metastasis.[17–19] Consequently, several radiomics studies have realized the magnitude of peritumoral zones for MVI prediction.[15,20,21] Usually, vascular invasion limits the implementation of curable treatments such as liver resection, transplantation and ablation, thus seriously threatening the outcomes of patients.[22–24] Hitherto, few prognostic radiomics studies[25–29] have focused on this highly aggressive domain. However, their studies[25–29] only investigated finite peritumoral regions, and did not extend to cover the three-dimensional volumetric interest (VOI) of the tumor and its periphery within 10 mm ($VOI_{tumor+10mm}$). Meanwhile, most of these researches were conducted by random grouping that reduced the reliability of the model versus n-fold cross-validation.

Accordingly, this study intended to develop a Gd-EOB-DTPA MRI-based peritumoral dilation radiomics with 5-fold cross-validation for preoperatively predicting 2-year recurrence in HCC patients without MaVI.

Methods

Study Population

This retrospective study was approved and exempted from written informed consent by the Ethical Review Committee of Zhongshan Hospital, Fudan University, Shanghai, China. Between March 2012 and June 2018, 323 pathologically confirmed HCC patients, who underwent preoperative Gd-EOB-DTPA MRI and hepatectomy in our hospital, were consecutively recruited into this research. The subject inclusion criteria was as follows (Figure 1A): (a) without MaVI, gross bile duct tumor thrombosis, lymph node or extrahepatic metastasis upon preoperative imaging; (b) without prior anti-tumor treatments; (c) completely clinicopathologic and follow-up data; (d) sufficient MRI quality within 1 month before liver resection. Among them, MaVI is defined as cancerous emboli in the gross vein and its corresponding main branches, which can be mostly detected by preoperative imaging modalities.[6,30] According to the Liver Imaging Reporting and Data System (LI-RADS),[31] the imaging definition of MaVI refers to the presence of unequivocal enhancing soft tissue in vein, regardless of visualization of parenchymal mass.

Biochemical and Histopathological Indicators

The preoperative biochemical metrics for predicting early relapse (Table 1) and overall recrudescence (Table S1) included the following indexes: serum alpha-fetoprotein (AFP), carcinoembryonic antigen, carbohydrate antigen 19–9, platelet, hepatitis B virus (HBV), anti-hepatitis C virus antibody, HBV-DNA load, alanine

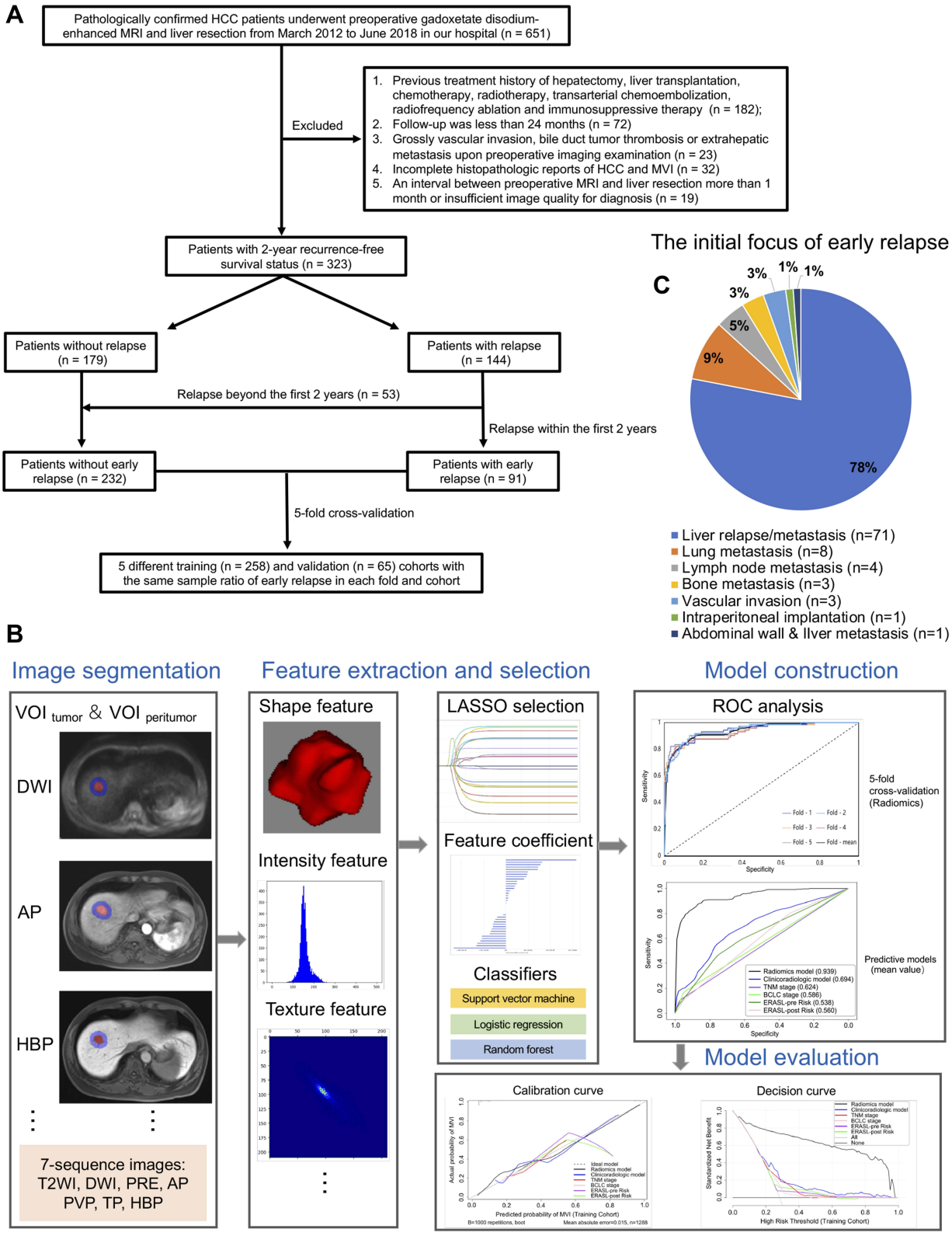

Figure 1 Flowchart of study population and radiomics analysis, as well as the first site of early recrudescence. Flowcharts (**A** and **B**) show the recruitment pathway of subjects and the technical route of radiomics analysis, respectively. Pie chart (**C**) summarizes the proportion of organs or tissues that are first involved in early recurrence. **Abbreviations**: HCC, hepatocellular carcinoma; MRI, magnetic resonance imaging; MVI, microvascular invasion; VOI, volumetric interest (volume of interest); DWI, diffusion weighted imaging; T2WI, T2-weighted imaging; PRE, pre-contrast phase; AP, arterial phase; PVP, portal venous phase; TP, transitional phase; HBP, hepatobiliary phase; LASSO, Least absolute shrinkage and selection operator; ROC, receiver operating characteristic curve.

Table 1 Baseline Characteristics for Predicting Early Recurrence

Variables	Without Early Recurrence (n=232)	Early Recurrence (n=91)	Univariable Logistic Regression		Multivariable Logistic Regression	
			OR (95% CI)	P	OR (95% CI)	P
Age(y, mean ± SD)	54.30 ± 10.893	55.38 ± 11.266	1.009(0.987,1.032)	0.426		
Sex(Male/Female)	203(62.8)/29(9.0)	77(23.8)/14(4.3)	0.786(0.394–1.566)	0.493		
HBV or HCV †	207(64.1)/25(7.7)	75(23.2)/16(5.0)	0.566(0.287–1.118)	0.101		
HBV-DNA (>10^4/≤10^4)	28(9.3)/190(63.3)	17(5.7)/65(21.7)	1.775(0.913–3.452)	**0.091**		
ES (III–IV/I–II)	84(26.0)/148(45.8)	44(13.6)/47(14.6)	1.649(1.010–2.694)	**0.046**		
Cirrhosis †	149(46.1)/83(25.7)	58(18)/33(10.2)	0.979(0.591–1.622)	0.934		
MVI †	50(15.5)/182(56.3)	38(11.8)/53(16.4)	2.610(1.550–4.394)	**<0.001**	2.132(1.122–4.050)	0.021
Ki-67	24.05 ± 17.787	27.49 ± 18.586	1.010(0.997–1.024)	0.124		
Size(>5cm/≤5 cm)	5(1.5)/227(70.3)	13(4.0)/78(24.1)	7.567(2.614–21.906)	**<0.001**	3.661(1.094–12.250)	0.035
Anatomical resection †	25(7.7)/207(64.1)	13(4.0)/78(24.1)	1.380(0.672–2.832)	0.380		
Multifocality(2–3/1 nodule) †	33(10.2)/199(61.6)	21(6.5)/70(21.7)	1.809(0.982–3.333)	**0.057**		
Satellite nodules †	1(0.3)/231(71.5)	4(1.2)/87(26.9)	10.621(1.171–96.345)	**0.036**		
AFP(>20/≤20 ng/mL) (>400/≤400 ng/mL)	96(29.7)/136(42.1) 25(7.7)/207(64.1)	48(14.9)/43(13.3) 14(4.3)/77(23.8)	1.581(0.971–2.575) 1.505(0.744–3.046)	**0.065** 0.255		
CEA (>5/≤5 ng/mL)	23(7.2)/206(64.6)	6(1.9)/84(26.3)	0.640(0.252–1.627)	0.348		
CA199(>34/≤34ng/mL)	40(12.5)/189(59.2)	22(6.9)/68(21.3)	1.529(0.848–2.756)	0.158		
TP(≤65/>65 g/L)	63(19.5)/169(52.3)	22(6.8)/69(21.4)	0.855(0.488–1.498)	0.585		
ALB(≤35/>35g/L)	4(1.2)/228(70.6)	3(0.9)/88(27.2)	1.943(0.426–8.858)	0.391		
TBA(>10/≤10 umol/L)	82(26)/145(46)	39(12.4)/49(15.6)	1.407(0.853–2.321)	0.181		
TBIL(>20.4/≤20.4 μmol/L)	24(7.4)/208(64.4)	14(4.3)/77(23.8)	1.576(0.775–3.202)	0.209		
DBIL(>6.8/≤6.8 umol/L)	43(13.3)/189(58.5)	22(6.8)/69(21.4)	1.401(0.782–2.511)	0.257		
ALT(>50/≤50 U/L)	29(9.0)/203(62.8)	24(7.4)/67(20.7)	2.232(1.203–4.140)	**0.011**	2.173(1.066–4.430)	0.033
AST(>40/≤40 U/L)	36(11.1)/196(60.7)	23(7.1)/68(21.1)	1.842(1.019–3.327)	**0.043**		
AKP(>125/≤125 U/L)	14(4.3)/218(67.5)	10(3.1)/81(25.1)	1.922(0.821–4.501)	0.132		
GGT(>60/≤60 U/L)	59(18.3)/173(53.6)	35(10.8)/56(17.3)	1.833(1.095–3.068)	**0.021**	1.941(1.062–3.548)	0.031
PLT(≤100/>100 x 10^9/L)	60(18.6)/171(53.1)	26(8.1)/65(20.2)	1.140(0.663–1.959)	0.635		
PT(>13.0/≤13.0 s)	30(9.3)/202(62.5)	14(4.3)/77(23.8)	1.224(0.616–2.432)	0.564		
PALB(≤250/>250mg/L)	165(51.1)/67(20.7)	74(22.9)/17(5.3)	1.768(0.971–3.217)	**0.062**	2.078(1.021–4.231)	0.044
ALBI(2/1 grade)	43(13.3)/189(58.5)	10(3.1)/81(25.1)	0.543(0.260–1.132)	0.103		
Non-smooth margin †	104(32.2)/128(39.6)	48(14.9)/43(13.3)	1.374(0.845–2.234)	0.200		
Nodule-in-nodule †	13(4.0)/219(67.8)	5(1.5)/86(26.6)	0.979(0.339–2.830)	0.969		
Fat suppression †	73(22.6)/159(49.2)	30(9.3)/61(18.9)	1.071(0.638–1.797)	0.795		
Necrosis †	61(18.9)/171(52.9)	24(7.4)/67(20.7)	1.004(0.579–1.741)	0.988		

(*Continued*)

Table 1 (Continued).

Variables	Without Early Recurrence (n=232)	Early Recurrence (n=91)	Univariable Logistic Regression		Multivariable Logistic Regression	
			OR (95% CI)	P	OR (95% CI)	P
Heterogenous T2WI †	67(20.7)/165(51.1)	27(8.4)/64(19.8)	1.039(0.610–1.768)	0.888		
Child-Pugh(B/A class)	9(2.8)/223(69.0)	6(1.9)/85(26.3)	1.749(0.604–5.062)	0.303		
BCLC						
0 stage	78(24.1)	18(5.6)	Reference	**0.020**		
A stage	142(44.0)	53(19.5)	1.923(1.063–3.476)	0.031		
B stage	12(3.7)	10(3.1)	3.611(1.351–9.654)	0.010		
TNM stage						
T1a	142(44.0)	37(11.5)	Reference	**0.001**		
T1b	33(10.2)	12(3.7)	1.396(0.657–2.964)	0.386		
T2	55(17.0)	38(11.8)	2.652(1.531–4.593)	0.001		
T3	2(0.6)	4(1.2)	7.676(1.353–43.535)	0.021		
ERASL-pre risk						
Low	227(70.3)	82(25.4)	Reference	**0.019**		
Intermediate	4(1.2)	8(2.5)	5.537(1.624–18.876)	0.006		
High	1(0.3)	1(0.3)	2.768(0.171–44.769)	0.473		
ERASL-post risk						
Low	220(68.1)	74(22.9)	Reference	**0.002**		
Intermediate	11(3.4)	16(5.0)	4.324(1.921–9.736)	<0.001		
High	1(0.3)	1(0.3)	2.973(0.184–48.128)	0.443		
Hemorrhage †	34(10.5)/198(61.3)	18(5.6)/73(22.6)	1.436(0.764–2.699)	0.261		
Mosaic architecture †	10(3.1)/222(68.7)	12(3.7)/79(24.5)	3.372(1.402–8.111)	**0.007**		
Targetoid architecture †	15(4.6)/217(67.2)	7(2.2)/84(26.0)	1.206(0.475–3.061)	0.694		
Non-rim APHE †	188(58.2)/44(13.6)	72(22.3)/19(5.9)	0.887(0.485–1.620)	0.696		
Non-peripheral washout †	179(55.4)/53(16.4)	77(23.8)/14(4.3)	1.628(0.853–3.109)	0.139		
Capsule enhancement						
Intact	139(43.0)	40(12.4)	Reference	**0.007**		
Incomplete	44(13.6)	32(9.9)	2.527(1.42–4.493)	0.002		
Absent	49(15.2)	19(5.9)	1.347(0.713–2.545)	0.358		
Peritumoral enhancement †	67(20.7)/165(51.1)	45(13.9)/46(14.2)	2.409(1.462–3.970)	**0.001**	1.826(0.989–3.374)	0.054
Peritumoral hypointensity †	50(15.5)/182(56.3)	33(10.2)/58(18.0)	2.071(1.219–3.517)	**0.007**		
HBP hypointensity †	225(69.7)/7(2.2)	90(27.9)/1(0.3)	2.800(0.340–23.084)	0.339		
Ascite †	15(4.6)/217(67.2)	6(1.9)/85(26.3)	1.021(0.383–2.719)	0.967		
Li-RADS						
LR-3	30(9.3)	9(2.8)	Reference	0.725		
LR-4	60(18.6)	23(7.1)	1.278(0.527–3.101)	0.588		
LR-5	142(44.0)	59(18.3)	1.385(0.620–3.096)	0.427		

Notes: †Presence/absence; P values in bold indicated that the corresponding variables were closely related to 2-year recurrence in the univariable logistic regression (P <0.1).
Abbreviations: OR, odd ratio; CI, confidence interval; HBV, hepatitis B virus; HCV, hepatitis C virus; HBV-DNA, deoxyribonucleic acid of hepatitis B virus; ES, Edmondson-Steiner grade; MVI, microvascular invasion; AFP, alpha-fetoprotein; CEA, carcinoembryonic antigen; CA199, carbohydrate antigen 19-9; TP, Total protein; ALB, albumin; TBA, total bile acid; TBIL, total bilirubin; DBIL, direct bilirubin; ALT, alanine aminotransferase; AST, aspartate aminotransferase; AKP, alkaline phosphatase; GGT, γ-glutamyl transpeptidase; PLT, platelet; PT, prothrombin time; PALB, prealbumin; ALBI, the albumin-bilirubin grade; T2WI, T2-weighted image; BCLC, the Barcelona Clinic Liver Cancer staging system; TNM, the American Joint Committee on Cancer tumor-node-metastasis system; ERASL-pre risk, ERASL-post risk, the preoperative and post-operative risks of Early Recurrence After Surgery for Liver tumor; APHE, arterial phase hyperenhancement; HBP, hepatobiliary phase; Li-RADS, the Liver Imaging Reporting And Data System.

aminotransferase (ALT), aspartate aminotransferase, total bilirubin, direct bilirubin, total protein, albumin, alkaline phosphatase, γ-glutamyltransferase, prealbumin, prothrombin time, and the Child-Pugh grade.

Histopathological characteristics (tumor size, number, necrosis, MVI, MaVI, satellite nodules, Ki-67 protein expression, gross bile duct cancer embolus, Edmondson–Steiner and liver fibrosis grades) were assessed in consensus by two experienced abdominal pathologists. Tumor stage was classified by the Barcelona Clinic Liver Cancer (BCLC) staging system,[1] the American Joint Committee on Cancer tumor-node-metastasis (TNM) system,[32] the preoperative and postoperative risks of Early Recurrence After Surgery for Liver tumor (ERASL-pre risk, ERASL-post risk),[33] respectively.

Gd-EOB-DTPA MRI

Each eligible subject underwent a 1.5-Tesla MRI scanner (Magnetom Aera, Siemens Healthcare, Erlangen, Germany), with intravenous injection of Gd-EOB-DTPA (0.025 mmol/kg, nearly 1.5 mL/s, flushed with 20-mL saline). Transversal sequences included into this research are given below: breath-hold fat-suppressed T2-weighted imaging (T2WI), free-breath diffusion-weighted imaging (DWI), dynamic fat-suppressed T1-weighted imaging with three-dimensional volumetric-interpolated breath-hold examination: pre- and post-contrasted phases (arterial phase: AP, 20–30 s, triggered automatically when Gd-EOB-DTPA reached the ascending aorta; portal venous phase: PVP, 60–70 s; transitional phase: TP, 180 s; hepatobiliary phase: HBP, 20 min). Detailed parameters of the above seven sequences are elaborated in Table S2.

Conventional Imaging Indicators

Only being informed of HCC lesions, two experienced radiologists independently evaluated tumor hallmarks as follows: size, number, non-smooth tumor edge, fat deposition, necrosis, hemorrhage, heterogeneous T2WI, nodule-in-nodule architecture,[31] mosaic architecture,[31] targetoid architecture,[31] peritumoral enhancement on AP images,[18] non-rim arterial phase hyperenhancement,[31] non-peripheral washout,[31] capsule enhancement on PVP/TP images,[34] peritumoral hypointensity on HBP images,[18] the classification of LI-RADS.[31] In case of any divergences, a consensus was reached after considerable debate. Typical Gd-EOB-DTPA MRI of early recurrence is illustrated in Figure 2.

Radiomics Analysis

Radiomic analysis was performed with uAI Research Portal (United Imaging Intelligence, China) that was embedded into the widely used package—PyRadiomics (https://pyradiomics.readthedocs.io/en/latest/index.html).[35–37] The workflow of radiomics was consisted of image segmentation, feature extraction, feature selection, model construction and evaluation (Figure 1B).

To avoid sample bias of grouping, our study population was implemented with the method of five-fold cross-validation.[38,39] More precisely, the whole population was randomly but equally divided into five partitions, with the same ratio of recurrence-free patients in each partition; training and validation were tested on four-fifths of population and the remaining partition, respectively. On the premise that each subject was used as validation data exactly once, the above two steps were randomly repeated five times. Consequently, it generated five different folds —five unlike training and validation cohorts, based on which an average but robust estimation could be obtained.

Tumor Segmentation and Feature Extraction

By means of ITK-SNAP software (http://www.itksnap.org/pmwiki/pmwiki.php), the three-dimensional segmentation of the whole tumor was manually and independently delineated by two radiologists on all 7-sequence axial images. Referring to previous studies, radiomics approach based on $VOI_{tumor+10mm}$ was superior to that of VOI_{tumor} in identifying MVI,[15,20,21] and MVI is a well-established risk factor for postoperative recrudescence.[30,40,41] Hence, the VOI of our peritumoral dilation radiomics was determined as $VOI_{tumor+10mm}$ after the radiologists' adequate discussion, in order to contain the effective bi-regional (tumor and peritumoral areas) signatures but limit the potential impact of redundant extrahepatic tissues on prognosis. Exactly, $VOI_{tumor+10mm}$ was obtained as follows: the manually outlined tumor contour on the binary images was automatically expanded by 10 mm through the widely used radiomics technology—the morphological dilation operation in three dimensions.[15,20,40,42,43]

Based on the original MR images, 118 signatures (Table S3) were extracted from the following feature categories: the first-order statistics, shape and size, Gray-Level Co-occurrence Matrix, Gray-Level Run-Length Matrix, Gray-Level Size-Zone Matrix, Gray-Level Dependence Matrix, and Neighboring Gray-Tone Difference Matrix. Meanwhile, 25 imaging filters (eg, Wavelets, Gaussian, Laplacian Sharpening) provided by uAI Research Portal

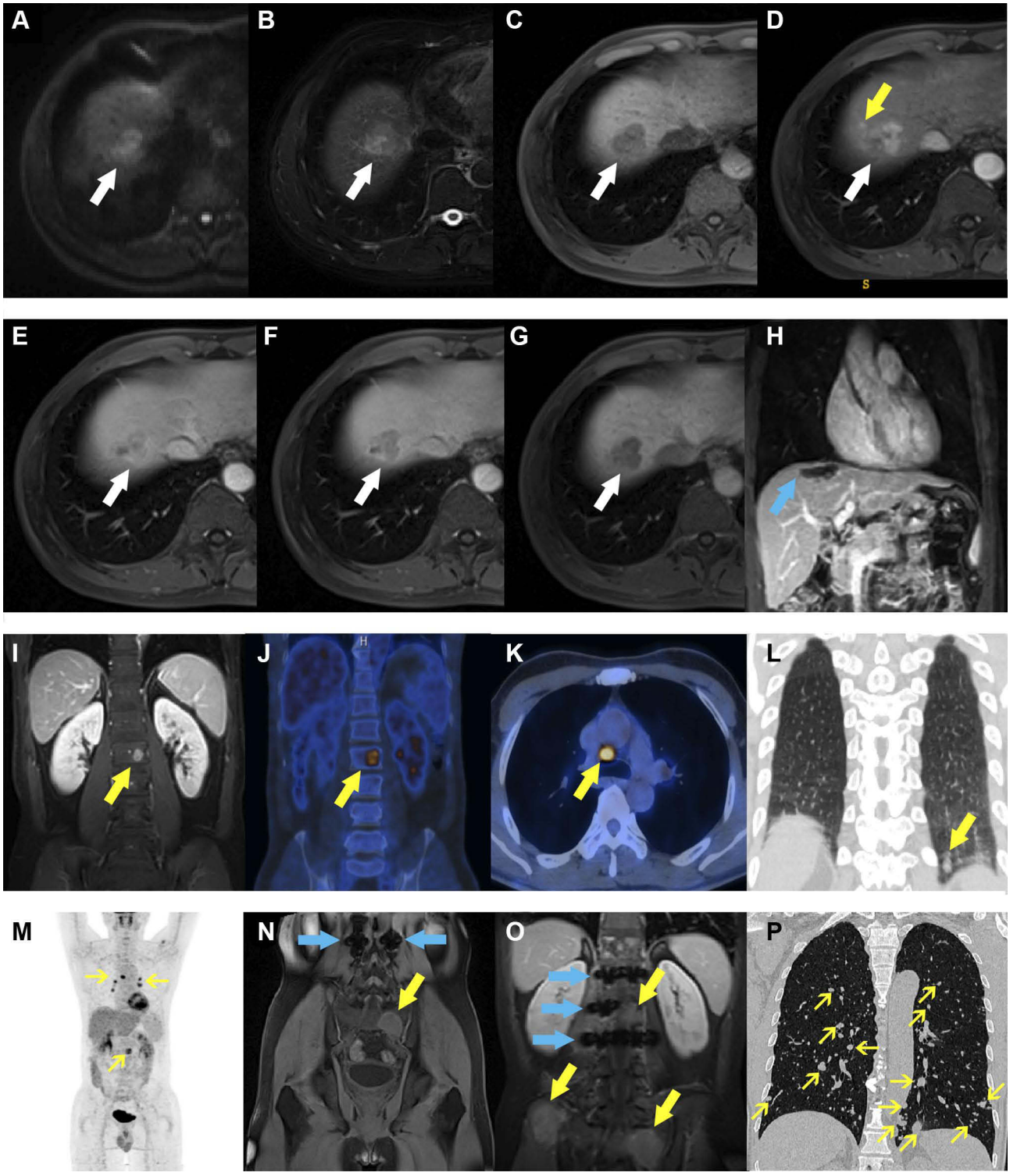

Figure 2 Representative images of early recurrence in patients with hepatocellular carcinoma after liver resection. A 59-year-old male with abnormal levels of alpha-fetoprotein, alanine aminotransferase, γ-glutamyltransferase, and prealbumin (34.4 ng/mL, 69 U/L, 67 U/L, and 160 mg/L) was admitted to our hospital for abdominal discomfort. Preoperative Gd-EOB-DTPA MRI detected a 3.1-cm lesion (**A**–**G**, white arrows) in hepatic segment VII, with typical architectures of hepatocellular carcinoma (HCC): hyperintensity on diffusion-weighted imaging (**A**), slight hyperintensity on T2-weighted imaging (**B**), slight hypointensity on pre-contrasted T1-weighted imaging (**C**), wash-in and wash-out on post-contrasted sequences (**D**–**F**, arterial, portal venous and transitional phases), and hypointensity on hepatobiliary phase (**G**). Peritumoral enhancement, an independent risk factor of 2-year relapse in our study, was only present on arterial phase image (**D**, yellow arrow) but absent on the other sequences. After hepatectomy (**H**, blue arrow, the domain of the liver parenchyma defect after liver resection), the lesion was pathologically confirmed to be HCC with microvascular invasion. Postoperative follow-up presented that this subject suffered from extrahepatic recurrence (**I**–**P**, yellow arrows): (**I**) lumbar vertebra (at 6 months); (**J**–**M**) lumbar vertebra, mediastinal lymph nodes and left lung (at 9 months); (**N**) sacral bone (at 12 months); (**O**) lumbar vertebra, sacrum and ilium (at 18 months); (**P**) the whole lungs (at 24 months), despite of bone radiotherapy and systemic chemotherapy. Among them, the blue arrows on (**N** and **O**) graphs were MRI metal artifacts of lumbar internal fixators that were used to maintain spinal stability.

were also used for feature extraction. Combining 118 features with 25 imaging filters, 2950 features were ultimately extracted from each sequence images, whether in VOI_{tumor} subgroup or $VOI_{tumor+10mm}$ subgroup.

Feature Selection

Feature selection began by evaluating the inter-delineator reproducibility. More concretely, the inter-correlation coefficient less than 0.8 was utilized to remove the unstable features. After normalization of Z-score, each stable feature was further selected by the least absolute shrinkage and selection operator regression (LASSO). According to the Harrell's guideline, the amount of selected features should be less than 10% of the sample size. As a result, the final number of features is approximately 30 in the experiment of the single sequence, multi-sequence fusion and the final radiomics model.

Model Construction

With P value less than 0.1 in the univariable logistic regression, the conventional image indicators evaluated by radiologists and clinicopathological indexes were enrolled into the multivariable logistic regression (backward stepwise: ward) for identifying independent predictors and developing the clinicoradiologic model.

Radiomics modeling began with the single sequence analysis to determine the better performance between VOI_{tumor} and $VOI_{tumor+10mm}$, as well as their performance ranking in each sequence. According to the predictive accuracy, single sequences in the better VOI subgroup were successively integrated to identify the best multi-sequence fusion (Tables 2 and S4). For maximizing radiomics algorithm's discrimination, the machine-learning classifiers of logistic regression, random forest and support vector machine (SVM) were implemented to model construction, respectively.

On the basis of the optimal radiomics model, each subject could derive an individualized radiomics score to predict early relapse. Subsequently, the radiomics score was incorporated with independent clinicoradiologic predictors to build the comprehensive nomogram.

Model Evaluation

In terms of model evaluation, the discrimination was firstly quantified with the area under the curve (AUC) of receiver operating characteristic (ROC). Afterwards, the calibration curve was used to estimate the coincidence between the prediction model and the actual outcomes. Finally, the decision curve with net reclassification improvement (NRI) was utilized to visualize the clinical net benefit of prediction models. NRI > 0 is a positive improvement and indicates that the predictive efficiency of the new model precedes that of the old one.

Follow-Up

Mainly based on serum tumor markers and imaging examinations, consistent follow-up was performed at intervals of 3 to 6 months after curative resection. Patients were censored on June 30, 2020. The date of hepatectomy, recrudescence, death and endpoints were recorded for calculating 2-year recurrence-free survival (RFS). Relapse was identified as de novo tumor (s) in the remnant liver or extrahepatic metastasis via the radiological or pathological examination.

Statistical Analysis

Statistical analyses were applied with IBM SPSS Statistics (version 25; IBM Corporation, Armonk, NY, USA) or R (version 3.6.1, https://www.r-project.org) software. $P<0.05$ was considered as statistically significant. Sample size was calculated by PASS software (version 15; NCSS, LLC, USA). According to the similar prognostic studies,[3,33] the 2-year relapse rate of HCC after liver resection was 30.0–43.0% (7 different centers, 1636/4797 recurrent patients in total). Hence, the parameters of ROC were set as follows: two-sided test, power of 0.9, alpha of 0.05, the targeted AUC of 0.8, and the population ratio of 1.3–2.3 (non-early recurrence to early relapse).

Results

Clinicoradiologic Characteristics and Their Prognostic Performances

As of June 30, 2020, 323 consecutive patients met with the inclusion criteria. After sample size calculation, the overall population, and the patients with early relapse or not fluctuated between 35–43, 13–15 and 20–30, respectively. Therefore, the number of our patients is far enough to meet the needs of diagnosis. In aggregate, the mean follow-up was 45.9 ± 20.5 (range 24–100) months and the median RFS reached 60.4 (95% CI 42.8–78.1) months. Cumulatively, 28.2% (91/323) and 16.4% (53/323) patients developed early and late recrudescence, respectively.

With regards to early recurrence, the baseline contexts of patients and the first site of recrudescence are summarized in Table 1 and Figure 1C, respectively. Among them, 78% (71/91) patients initially suffered from remnant liver

Table 2 The Mean Performances of Diverse Sequences After 5-Fold Cross-Validation† for Predicting 2-Year Relapse

Volumetric Interest (VOI)	Sequences (Feature Number)	Training Dataset (n = 258)				Validation Dataset (n = 65)			
		Sen	Spe	Acc	AUC (95% CI)	Sen	Spe	Acc	AUC (95% CI)
VOItumor	T2 (32)	0.422	0.936	0.797	0.804(0.744–0.866)	0.329	0.909	0.746	0.738(0.598–0.882)
	DWI (21)	0.343	0.926	0.762	0.769(0.705–0.835)	0.296	0.892	0.723	0.648(0.493–0.805)
	PRE (20)	0.256	0.952	0.755	0.724(0.654–0.795)	0.198	0.948	0.736	0.663(0.515–0.814)
	AP (22)	0.294	0.938	0.756	0.784(0.724–0.846)	0.253	0.922	0.733	0.720(0.583–0.859)
	PVP (28)	0.135	0.989	0.748	0.721(0.654–0.789)	0.111	0.987	0.739	0.673(0.532–0.817)
	TP (24)	0.459	0.948	0.810	0.846(0.796–0.897)	0.363	0.935	0.773	0.764(0.641–0.888)
	HBP (22)	0.368	0.952	0.787	0.777(0.714–0.842)	0.275	0.909	0.730	0.645(0.490–0.802)
	7 sequences (41)	0.662	0.972	0.884	0.927(0.891–0.968)	0.494	0.909	0.792	0.823(0.714–0.936)
VOItumor+1cm	T2 (33)	0.357	0.395	0.763	0.800(0.745–0.859)	0.395	0.904	0.761	0.722(0.586–0.860)
	DWI (20)	0.415	0.932	0.785	0.787(0.724–0.849)	0.385	0.900	0.754	0.715(0.578–0.853)
	PRE (25)	0.278	0.951	0.761	0.764(0.702–0.827)	0.265	0.939	0.749	0.710(0.574–0.853)
	AP (25)	0.494	0.950	0.821	0.840(0.788–0.894)	0.374	0.909	0.758	0.748(0.617–0.881)
	PVP (22)	0.365	0.944	0.78	0.779(0.718–0.842)	0.308	0.922	0.748	0.696(0.556–0.837)
	TP (22)	0.302	0.942	0.761	0.805(0.749–0.860)	0.264	0.926	0.739	0.735(0.608–0.863)
	HBP (24)	0.503	0.935	0.813	0.838(0.786–0.891)	0.427	0.900	0.767	0.729(0.589–0.870)
	HBP+T2 (38)	0.527	0.947	0.828	0.881(0.836–0.928)	0.429	0.926	0.786	0.764(0.635–0.897)
	HBP+T2+AP (33)	0.720	0.995	0.917	0.988(0.985–0.999)	0.385	0.965	0.801	0.769(0.635–0.918)
	HBP+T2+DWI (39)	0.585	0.960	0.854	0.899(0.855–0.947)	0.450	0.913	0.783	0.752(0.616–0.889)
	HBP+T2+DWI+AP (33)	0.368	0.978	0.806	0.839(0.784–0.897)	0.307	0.948	0.767	0.723(0.583–0.855)
	7 sequences (38)	0.736	0.961	0.898	0.939(0.908–0.973)	0.604	0.909	0.823	0.842(0.736–0.951)

Note: †The trained and validated performances of each fold for predicting early recurrence is elaborated in Table S4.

Abbreviations: Sen, sensitivity; Spe, specificity; Acc, accuracy; AUC, area under receiver operating characteristic curve; CI, confidence interval; T2, T2-weighted imaging; DWI, diffusion-weighted imaging; Pre, pre-contrasted phase; AP, arterial phase; PVP, portal venous phase; TP, transitional phase; HBP, hepatobiliary phase; VOItumor, the three-dimensional volume of the whole tumor; VOItumor+1cm, the volumetric interest of the whole tumor and the adjacent liver area within 1 cm from the tumor edge.

relapse/metastasis. By the multivariable logistic regression, MVI (OR 2.132, 95% CI: 1.122–4.050, P = 0.021), tumor size >5 cm (OR 3.661, 95% CI: 1.094–12.25, P = 0.035), ALT >50 U/L (OR 2.173, 95% CI: 1.066–4.430, P = 0.033), γ-glutamyltransferase >60 U/L (OR 1.941, 95% CI: 1.062–3.548, P = 0.031), prealbumin ≤250 mg/L (OR 2.078, 95% CI: 1.021–4.231, P = 0.044) and peritumoral enhancement (OR 1.826, 95% CI: 0.989–3.374, P = 0.054) were independently susceptible to early recurrence and yielded a moderate predictive performance (AUC: 0.694, 95% CI: 0.628–0.760, P<0.001).

$$Y = -2.448 + 1.298\,tumor\,size + 0.776ALT + 0.757\,MVI + 0.732\,prealbumin + 0.663\gamma - glutamyltransferase + 0.602\,peritumoral\,enhancement$$

Furthermore, our clinicoradiologic model outperformed the TNM stage (AUC: 0.623, 95% CI: 0.553–-0.693; P = 0.001), BCLC classification (AUC: 0.585, 95% CI: 0.517–0.653, P = 0.018), ERASL-post risk (AUC: 0.567, 95% CI: 0.495–0.640, P = 0.059) and ERASL-pre risk (AUC: 0.539, 95% CI: 0.467–0.610, P = 0.281) in 2-year recurrence prediction.

As for the overall recurrence, the demographics characteristics of patients are shown in Table S1. Multivariable Cox regression demonstrated that tumor size >5 cm (HR 3.749, 95% CI 2.082–6.752, P<0.001), peritumoral enhancement (HR 1.914, 95% CI 1.327–2.760, P = 0.001), ALT >50 U/L (HR 1.782, 95% CI 1.151–2.761, P = 0.010), and alkaline phosphatase >125 U/L (HR 2.142, 95% CI 1.193–3.848, P = 0.011) independently impaired the outcomes, with a similar unsatisfactory AUC of 0.723 (95% CI 0.659–0.786, P<0.001).

Given these ill-distinguishably clinical models, we turned to investigate peritumoral dilation radiomics with 5-fold cross-validation for improving prediction.

Prognostic Performance of Peritumoral Dilation Radiomics

After 5-fold cross-validation, the mean validated accuracy of VOI_{tumor} in each single-sequence radiomics approach was inferior to that of $VOI_{tumor+10mm}$ (Table 2), and HBP showed the most effective accuracy for early relapse in the $VOI_{tumor+10mm}$ subgroup. Subsequently, single sequences of $VOI_{tumor+10mm}$ based on the mean validated accuracy were successively fused to achieve the optimal integration. Namely, multi-sequence fusion experiments began with HBP at $VOI_{tumor+10mm}$. Nevertheless, the average AUCs of multi-sequence models (up to 4 sequences) only fluctuated from 0.723 to 0.769 in the validation cohort, which slightly outperformed those of single sequences or clinical models. Hence, we altered the original intention of establishing an optimal multi-sequence integration.

Instead of fusing satisfactory sequences, 171 signatures selected from 7-sequence images in the previous single sequence analysis (Table S4) were regarded as new candidate feature sets. Based on the dimension reduction of LASSO, 38 highest RFS-correlated signatures (Table S5 and Figure S1) was tailored as the best 7-sequence feature subset. It was then used for modeling by SVM, logistic regression, and random forest, respectively. After 5-fold cross validation, SVM (the kernel function: radial basis function; the gamma parameter: 0.01) yielded the best performance for identifying 2-year recurrence, which was denoted as the optimal radiomics model. The mean AUC of this radiomics algorithm reached 0.939 (95% CI 0.908–0.973) in the training subgroup and 0.842 (95% CI 0.736–0.951) in the validation cohort. Meanwhile, the 7-sequence accuracy and AUC of $VOI_{tumor+10mm}$ also exceeded those of VOI_{tumor} in both training and validation sets after 5-fold cross-validation. The corresponding ROC of $VOI_{tumor+10mm}$ in each fold is plotted in Figure S2, and the six most distinguishing features of this optimal radiomics model are explicated in Table S6.

Most notably, our 7-sequence $VOI_{tumor+10mm}$ radiomics obtained the optimal average AUC (Table 3; Figure 3A and B), consistency with the actual 2-year relapse (Figure

Table 3 The Mean Discriminations of Diverse Models After 5-Fold Cross-Validation for Identifying 2-Year Recrudescence

Model	Training Cohort (n = 258)			Validation Cohort (n = 65)		
	AUC (95% CI)	NRI	P (NRI)	AUC (95% CI)	NRI	P (NRI)
Radiomics	0.939(0.908–0.973)	61.8%	<0.001	0.842(0.736–0.951)	51.3%	<0.001
Clinicoradiogic	0.694(0.660–0.726)	7.3%	0.004	0.707(0.627–0.759)	15.5%	0.002
TNM stage	0.624(0.590–0.659)	9.4%	0.007	0.626(0.555–0.694)	13.7%	0.041
BCLC stage	0.586(0.551–0.620)	1.9%	0.347	0.587(0.517–0.654)	8.2%	0.209
ERASL-pre risk	0.538(0.503–0.574)	−4.3%	0.990	0.538(0.467–0.610)	1.9%	0.268
ERASL-post risk	0.560(0.531–0.604)	Ref	Ref	0.529(0.495–0.640)	Ref	Ref
Radiomics vs Clinicoradiologic	/	54.5%	<0.001	/	35.9%	<0.001
Radiomics vs TNM stage	/	52.4%	<0.001	/	37.7%	<0.001
Radiomics vs BCLC stage	/	59.8%	<0.001	/	43.2%	<0.001
Radiomics vs ERASL-pre risk	/	66.1%	<0.001	/	49.4%	<0.001

Abbreviations: AUC, area under receiver operating characteristic curve; CI, confidence interval; NRI, net reclassification improvement; Ref, reference; BCLC, the Barcelona Clinic Liver Cancer staging system; TNM, the tumor-node-metastasis system; ERASL-pre and ERASL-post risk, the preoperative and postoperative risks of Early Recurrence After Surgery for Liver tumor.

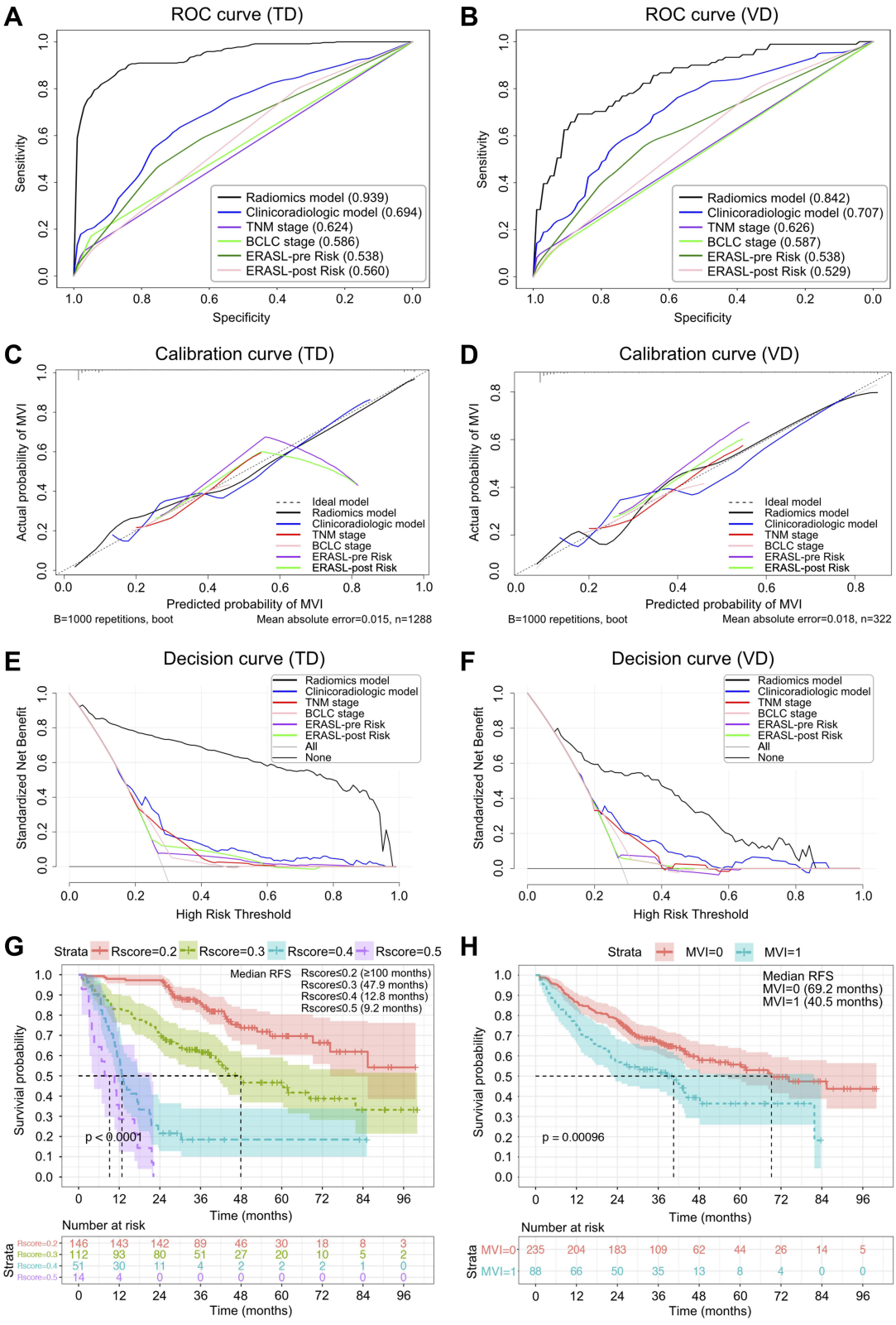

Figure 3 Receiver operating characteristic, calibration, and decision curves of early recrudescence, and Kaplan–Meier curves for the overall recurrence. The receiver operating characteristic (**A** and **B**), calibration (**C** and **D**), and decision (**E** and **F**) curves of different models for predicting early relapse in the training dataset (TD) and validation dataset (VD). With the 2-sided Log rank test, Kaplan–Meier curves of the overall recurrence were scaled by radiomics score (R-score ≤0.2, ≤0.3, ≤0.4, and ≤0.5; (**G**) and microvascular invasion (MVI, non-MVI; (**H**), respectively.

3C and D) and clinical net benefit (Figure 3E and F) in the training and validation cohorts, followed by the clinicoradiologic model, TNM classification, BCLC stage, ERASL-pre and ERASL-post risks. Concretely, NRIs further signified significant improvements of radiomics model versus the five clinical algorithms, either in the training cohort (NRIs: 52.4%-66.1%, P <0.001) or in the validation cohort (NRIs: 35.9%-51.3%, P <0.001). Furthermore, the Kaplan–Meier curve of this peritumoral dilation radiomics and MVI states excellently stratified HCC outcomes (Figure 3G and H, Log rank test, P <0.001): the higher grade of radiomics score, the higher risk of the overall recrudescence; the MVI-positive status significantly impaired the recurrence-free survival.

Prognostic Performance of the Comprehensive Nomogram

In terms of the comprehensive nomogram, our radiomics score possessed an overwhelming predominance (OR 4.1 × 10^{11}, P <0.001; Table S7) in the multivariate analysis for early relapse. However, the aforementioned clinicoradiologic factors (MVI, ALT, γ-glutamyltransferase, prealbumin, and peritumoral enhancement) failed to derive robust and independent performances (all P values >0.05) in the procedure. The heatmap (correlation matrix) between the 38 features of the optimal radiomics model and all clinicoradiologic characteristics for predicting early recurrence is illustrated in Figure 4. Although the integrated nomogram (Figure 5; AUC 0.914, 95% CI 0.880–0.947) slightly excelled the radiomics algorithm (AUC 0.909, 95% CI 0.875–0.943) in all population, we still regarded the peritumoral dilation radiomics as the ultimate prediction model of early recurrence.

Apart from our radiomics findings, Table 4 also summarizes the comparison of previous radiomics studies based on Gd-EOB-DTPA MRI[15,27–29,43–46] for predicting MVI or prognosis, as well as that of peritumoral dilation radiomics researches conducted by CT or MRI without hepatobiliary-specific agent for stratifying outcomes.

Discussion

This study developed a peritumoral deliration radiomics of Gd-EOB-DTPA MRI by 5-fold cross-validation, and derived a satisfying discrimination of 2-year recurrence in HCC patients without MaVI. Notably, our radiomics model revealed marked enhancements versus the clinicoradiologic algorithm, TNM stage, BCLC classification, ERASL-pre and ERASL-post risks for identifying early relapse, with NRIs reaching 35.9%-66.1%. To our knowledge, no radiomics study has associated peritumoral dilation algorithm of $VOI_{tumor+10mm}$ with outcomes in HCC patients after liver resection.

Peritumoral parenchyma harbors highly invasive tumor cells,[17] and preoperative identification of predisposing predictors for early relapse is crucial for stratifying patient risk, performing prompt intervention and improving long-term survival.[5,25,46] Hence, we initially constructed a clinicoradiologic model embodying peritumoral hallmarks/behaviours to predict early recurrence. The results demonstrated that MVI, peritumoral enhancement, tumor size >5cm, ALT >50 U/L, γ-glutamyltransferase >60 U/L and prealbumin ≤250 mg/L independently impaired 2-year RFS.

Previous studies have reported that MVI[15,40,47,48] and peritumoral enhancement[5] shorten the RFS independently, confirming to our findings. Pathologically, MVI first and foremost involves the peritumoral parenchyma, and further serves as the major haematogenous dissemination pathway of satellite nodules, MaVI, intra- and extrahepatic metastasis.[18,19] Peritumoral enhancement, stemmed from compensatory arterial hyperperfusion, frequently occurs in domains of MVI.[34,49,50] Besides, vascular endothelial growth factor receptor (VEGFR) can favour pathologic angiogenesis and form abnormal vessels, thus potentiating MVI[51] and compensatory arterial hyperperfusion in peritumoral areas (ie, peritumoral enhancement). Similarly, the tumor–host interaction between MVI and VEGFR has been reported to exacerbate the progression of renal cell carcinoma.[52] Therefore, MVI correlated with peritumoral enhancement, implying biological heterogeneity and heterochrony of HCC progression, is essential for postoperative prophase monitoring.

Tumor size >5 cm,[3,48,53] decreased prealbumin,[54] elevated ALT[55,56] and γ-glutamyltranspeptidase values[57–59] are independently vulnerable to recrudescence, which is consensus on our results. Tumor size >5 cm signifies an obvious high incidence of MVI, MaVI, satellite nodules, positive surgical margins, elevated AFP levels, HCC rupture, poor differentiated neoplasm, and serious background liver (chronic hepatitis, fibrosis and cirrhosis).[60] These indexes are prone to recurrence or dismal outcome. Since most HCCs develop from inflammation-related hepatic diseases, prognostic estimation should include not only

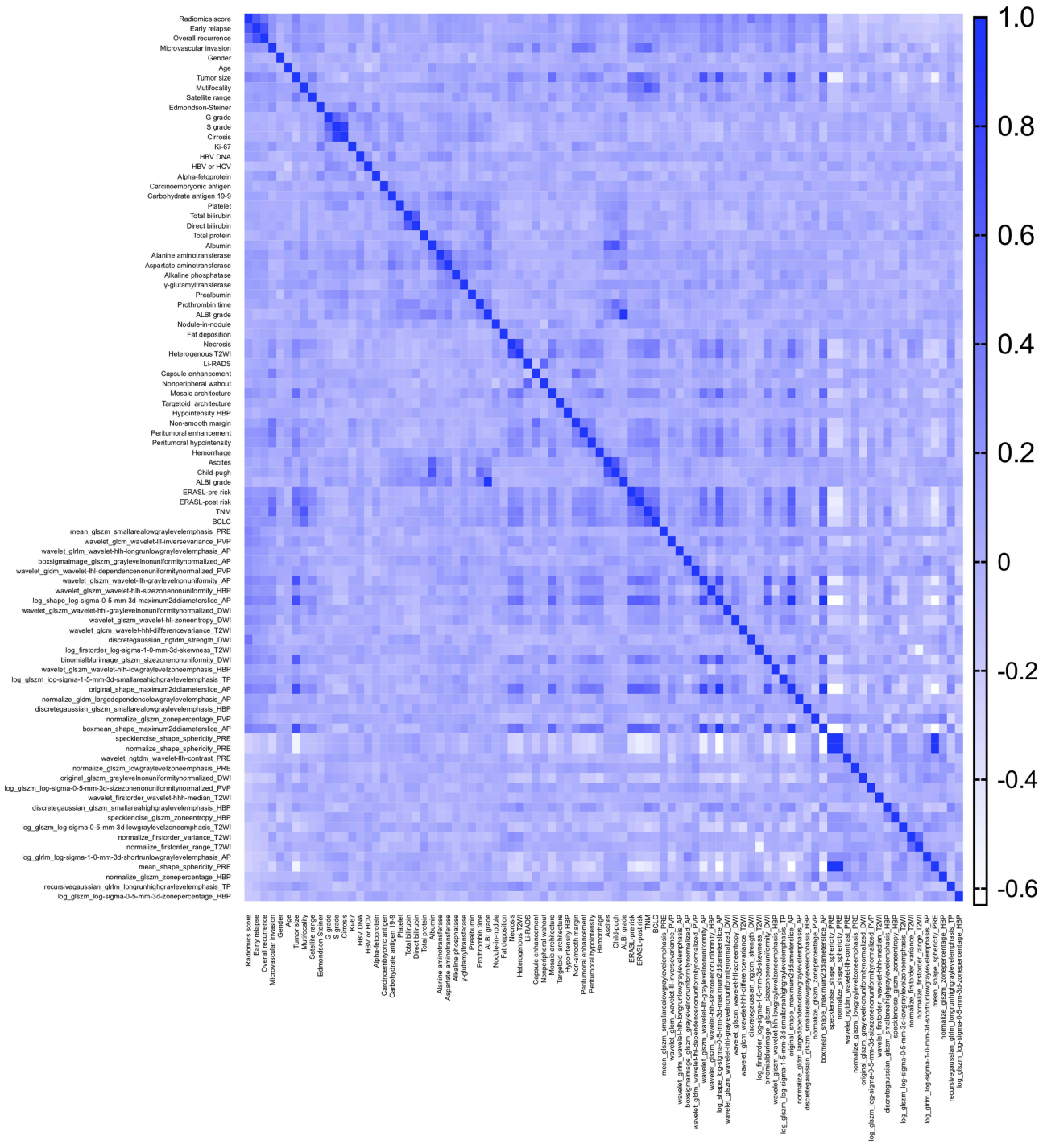

Figure 4 The heatmap between the 38 most recurrence-related features and baseline characteristics for predicting early recrudescence.
Abbreviations: HBV-DNA, deoxyribonucleic acid of hepatitis B virus; HBV, hepatitis B virus; HCV, hepatitis C virus; ALBI, the albumin-bilirubin grade; T2WI, T2-weighted image; LI-RADS, the Liver Imaging Reporting And Data System; HBP, hepatobiliary phase; ERASL-pre risk, ERASL-post risk, the preoperative and postoperative risks of Early Recurrence After Surgery for Liver tumor; TNM, the American Joint Committee on Cancer tumor-node-metastasis system, BCLC, the Barcelona Clinic Liver Cancer staging system; DWI, diffusion-weighted imaging; PRE, pre-contrasted phase; AP, arterial phase; PVP, portal venous phase; TP, transitional phase.

tumor size and behaviour but also hepatic function impairment that is easily detected before surgery.

However, the above clinicoradiologic indicators were paucity of robustness and only yielded a limited discrimination when incorporating with peritumoral dilation radiomics in early relapse assessment. Besides, our bi-regional radiomics was also superior to the clinicoradiologic model for 2-year recurrence after curative resection of An

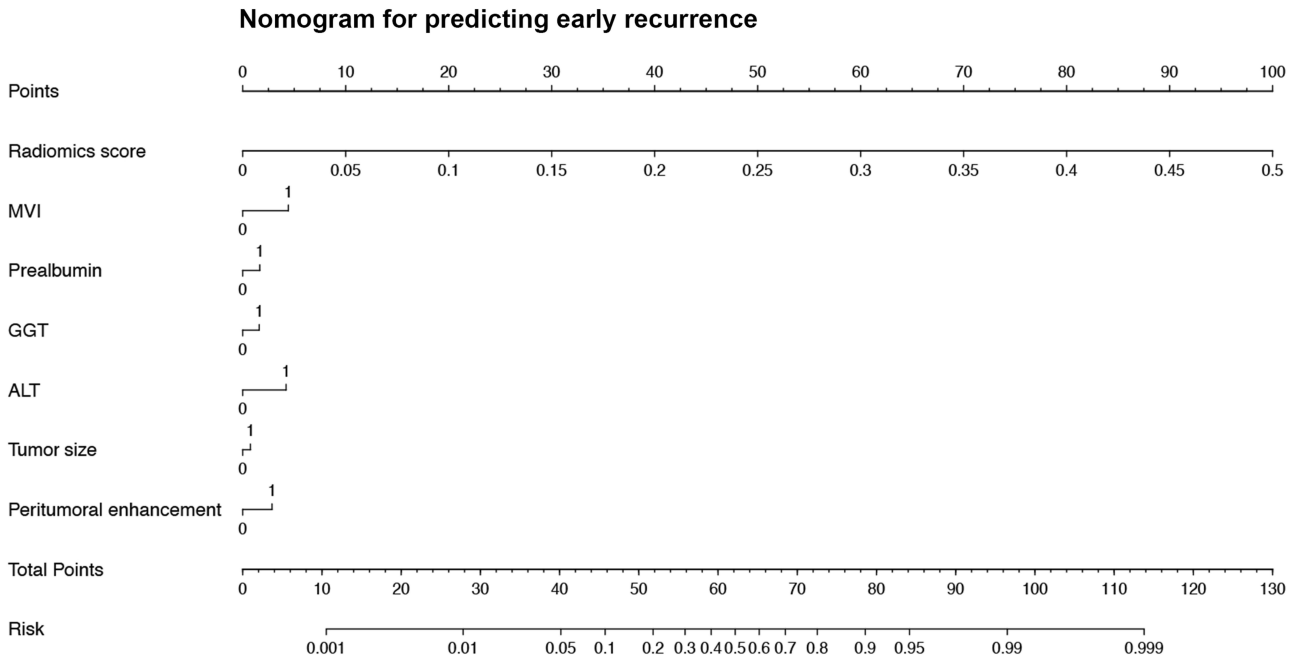

Figure 5 The nomogram of the comprehensive model for identifying early relapse in all population.
Abbreviations: ALT, alanine aminotransferase (0, ≤50 U/L; 1, >50 U/L); GGT, γ-glutamyltransferase (0, ≤60 U/L; 1: >60 U/L); prealbumin (0, >250 mg/L; 1, ≤250 mg/L), MVI, microvascular invasion (0, absent; 1, present); peritumoral enhancement (0, absent; 1, present).

et al study.[5] The reason may that our radiomics algorithm has merged high-dimensional signatures of peritumoral domains—high-hazard spreading scopes of MVI and satellite nodules.[17,61] Generally, satellite nodules are originated from MVI,[17] and a wide resection margin is recommended to MVI-positive HCCs for reducing the proportion of adverse outcomes.[15,49] However, MVI presents in 15–57.1% of HCC specimens and is only visible on microscopy.[15,17,62] Hence, we suppose that the patients with high-risk recurrence—preoperative high radiomics score can 1) properly enlarge resection margin or even adopt anatomical hepatectomy; 2) choose neoadjuvant therapy before surgery; 3) adhere to normative follow-up strategy.

Moreover, our $VOI_{tumor+10mm}$ might embody the high-throughput signatures of MVI high-risk zones. Thus, our prognostic prediction of $VOI_{tumor+10mm}$ radiomics model was better than those of Gd-EOB-DTPA MRI-based radiomics approaches using VOI_{tumor},[46] $VOI_{tumor+3mm}$,[29] $VOI_{tumor+5mm}$,[28] and $ROI_{tumor+10mm+liver}$.[27] Besides, HBP—the special phase of Gd-EOB-DTPA MRI—reflecting the expression of organic anion transporting polypeptide (OATP) is closely correlated with tumorigenesis and development.[7,63,64] During hepatocarcinogenesis, the declined expression of OATP was prior to the other key alterations (the increase of arterial flow and the decrease of portal venous flow).[63] That may be the reason that 1) compared with other single sequences in our $VOI_{tumor+10mm}$ subgroup, HBP showed the most effective prediction in the validation dataset for postoperative early recurrence; 2) our radiomics also outperformed the CT-based radiomics of $ROI_{tumor+20mm}$ for 2-year relapse after curative ablation or resection,[26] and even the non-hepatobiliary-specific MRI-based radiomics of VOI_{tumor} or $VOI_{tumor+5mm}$ for RFS prediction after transarterial chemoembolization.[25] Notably, $ROI_{tumor+20mm}$[26] or $ROI_{tumor+10mm+liver}$[27] was not a three-dimensional volume, but the largest cross-sectional area of tumor combined with its same layer of peritumoral parenchyma or the remaining liver, respectively. Meanwhile, the vast majority of aforementioned studies.[25–29,46] were calculated by random grouping, ignoring the interclass selective bias and reducing the reliability of algorithm to a certain degree.

The six top-ranked features of our final radiomics model implied oncologic behaviour. Intriguingly, four of six signatures were relevant to bi-regional heterogeneity as follows: Pre_glszm_SmallAreaLowGrayLevelEmphasis (SALGLE), AP_glszm_GrayLevelNonuniformityNormalized (GLNN), PVP_ gldm_DependenceNonuniformityNormalized (DNN) and PVP_glcm_InverseVariance. By definition, the higher value of SALGLE in pre-contrast images, GLNN in AP images, DNN or inverse variance in PVP images, the greater

Table 4 Comparison of Gd-EOB-DTPA MRI-Based Radiomics Studies for Predicting Microvascular Invasion and Prognosis, as Well as the Peritumoral Dilation Radiomics for Stratifying Prognosis

Radiomics Study		Volume or Region of Interest (VOI, ROI) for Radiomics Modeling	Sample Size (Data Source) and Grouping Method	AUC (Training/ Validation Dataset)	Sequence and Classifier for Radiomics Modeling	Tumor Number and Tumor Size Below 5 cm	BCLC Stage (0 and A)	Relationship Between MVI and Prognosis
Gd-EOB-DTPA MRI radiomics for MVI	Chong[15]	VOItumor+10mm+liver	356 (single center), 7:3†	0.960/0.920	HBP+PVP+AP +DWI, RF	Solitary(100%), 100%	100%	MVI – recurrence (2 years)*
	Feng[43]	VOItumor+10mm	160 (single center), 7:3†	0.850/0.833	HBP, LR	Solitary(71.9%), 69.4%	76.3%	NA
	Yang[44]	VOItumor	208 (single center), 7:3#	0.943/0.861	HBP+HBP T1 maps, LR	Solitary(82.7%), NA	NA	NA
	Zhang[45]	VOItumor	130 (single center), 7:3#	0.795 (10-fold cross-validation)	HBP, SVM	NA	NA	NA
Gd-EOB-DTPA MRI radiomics for prognosis after resection	Zhang[46]	VOItumor	155 (single center), 7:3#	0.844/0.841	HBP+AP+T2WI, LR	Solitary(65.2%), 43.9%	99.4%	VI-recurrence (1 year)*
	Kim[29]	VOItumor+3mm	167 (single center), 7.7:2.3	0.716 (validation)	HBP+AP+PVP, RF-Cox	Solitary (100%),100% (2–5cm)	94.0%	MVI – 2-year RFS*
	Zhang[28]	VOItumor+5mm	153 (single center), 7:3†	0.721/0.725	HBP+T2WI+PRE +AP, LASSO-Cox	NA	NA	MVI – RFS $
	Zhang[27]	ROItumor+10mm+liver	120 (single center), 7:3†	0.92/0.84	T2+PRE+AP +PVP+HBP, LASSO-Cox	Solitary(25%), 46.7%	60.0%	NA
	Our study	VOItumor+10mm	323 (single center), 5-fold cross-validation	0.939/0.842	7-sequence, SVM	Solitary(83.3%), 94.4%	93.2%	MVI– recurrence (2 years) $
MRI radiomics for prognosis after TACE	Song[25]	VOItumor	184 (single center), 6:4†	0.736/0.802	PVP, LASSO-Cox	Solitary(75.5%), 84.2%	90.8%	NA
CT radiomics for prognosis after ablation/resection (2:1)	Shan[26]	ROItumor+20mm	156 (single center), 7:3†	0.80/0.79	PRE+AP+PVP, LR	Solitary(76.9%), NA	NA	NA

Notes: †Random allocation; #assignment based on the date of preoperative MRI examination; *MVI or VI was determined to be an independent risk factor for early recurrence after liver resection; $when combined with the radiomics score, MVI was an important but not an independent risk factor for recurrence; Zhang et al[27,28,46] performed radiomics experiments on T2WI, PRE, AP, PVP, and HBP images, but did not include DWI and transitional phase (TP); meanwhile, Kim et al[29] only referred to radiomics experiments of AP, PVP and HBP, while neglected potential information of T2WI, DWI and TP; although Song et al[25] explored the peritumoral dilation radiomics models (VOItumor+1mm, VOItumor+3mm and VOItumor+5mm) on PVP images, the prediction efficiency of VOItumor was determined as the best one in the validation cohort; besides, the study of Song et al[25] was not derived from Gd-EOB-DTPA MRI, but gadodiamide-enhanced MRI without hepatobiliary-specific properties; most importantly, the region of interest concerned by Zhang et al[27] and Shan et al[26] was not a three-dimensional volume, but the largest cross-sectional area of tumor and its same layer of hepatic tissue; namely, the radiomics study of Zhang et al[27] investigated the performance of ROItumor+10mm+liver rather than VOItumor+10mm+liver, and Shan et al[26] focused on ROItumor+20mm instead of VOItumor+20mm.

Abbreviations: Gd-EOB-DTPA, Gadoxetate Disodium; MRI, magnetic resonance imaging; VOI, volume of interest; ROI, region of interest; AUC, area under receiver operating characteristic curve; BCLC, Barcelona Clinic Liver Cancer; MVI, microvascular invasion; VI, macro- or microvascular invasion; RFS, recurrence-free survival; T2WI, T2-weighted image; DWI, diffusion-weighted images; PRE, pre-contrast phase; AP, arterial phase; PVP, portal venous phase; HBP, hepatobiliary phase; RF, random forest; LR, logistic regression; TACE, transcatheter arterial chemoembolization; SVM, support vector machine; LASSO, least absolute shrinkage and selection operator; NA, not applicable, because it was not mentioned or investigated in the study.

complex chaos of the bi-region domain. Previous studies proposed that intratumoral heterogeneity might be induced by tumor cellularity, micronecrosis and inflammation, which might further facilitate MVI[15,49,65] and thus impair RFS. Furthermore, the elevation of GLNN in AP images is analogous to the mosaic architecture (intense intratumoral heterogeneity on AP) that was significantly susceptible to recurrence in our univariate analysis. Hence, our results are highly consistent with the well-known cognition: the greater heterogeneity, the more aggressive behavior, treatment-resistant and dismal prognosis.[66] Being alien to AP_glrlm_LongRunLowGrayLevelEmphasis (LRLGLE), HBP_glszm_ZonePercentage, a protective factor for recurrence, measures the coarseness of bi-regional texture, with higher value indicating more fine texture. In some sense, the two signatures are closely related to the roughness of tumor contour, implying an aggressive tendency to invade the cancerous envelope and protrude into the peritumoral non-neoplastic parenchyma. Moreover, rough/unsmooth tumor margin and incomplete/absent tumor capsule are well-recognized independent risk factors for MVI,[15,30,40,44] which will further trigger postoperative recrudescence.

Commonly, malignant lesions possess multi-domainal (eg, gross, cellular, genetic and phenotypic levels) and multi-dimensional (eg, cellular density, angiogenesis, hemorrhage and necrosis) heterogeneity,[66] which are finitely captured and quantified by the subjective interpretation of experienced radiologists. Just as a "virtual histopathology", our peritumoral dilation radiomics provides an objective and microcosmical high-throughput prognostication.

The limitation of this study firstly lies in the retrospective single-center scheme. Hence, the 5-fold cross-validation was implemented in our population for balancing the interclass biases. Furthermore, a prospective multicenter dataset should be utilized in the following research. Besides, given the preponderance of Gd-EOB-DTPA MRI, our oncological context mainly focused on tumor size ≤5 cm (94.4%). Accordingly, the reliability and robustness of our findings should be verified by larger HCCs.

Conclusions

Peritumoral dilation radiomics developed from the hepatobiliary-specific Gd-EOB-DTPA MRI is an excellent biomarker for early recrudescence of HCC, facilitating the non-invasive burgeon of individualized treatment and surveillance regimens.

Ethics Approval and Informed Consent

This retrospective study was conducted in accordance with the declaration of Helsinki (revised in 2013), which was approved and exempted from written informed consent by the Ethical Review Committee of Zhongshan Hospital, Fudan University, Shanghai, China. The reason for exemption of informed consent is that this non-invasive radiomics study is based on clinical history data related to previous diagnosis or treatment, and does not involve personal privacy and commercial interests. Specifically, all the original images were deleted from the subject's personal information (name, address, telephone number, hospitalization number, etc.), and then desensitized and encrypted for radiomics analysis. During the radiomics analysis, all imaging data was stored anonymously in our hospital database, with the anonymous code saved by our team leaders (Mengsu Zeng and Chun Yang).

Author Contributions

Huanhuan Chong and Yuda Gong share the first authorship of this paper.

All authors made a significant contribution to the work reported, whether that is in the conception, study design, execution, acquisition of data, analysis and interpretation, or in all these areas; took part in drafting, revising or critically reviewing the article; gave final approval of the version to be published; have agreed on the journal to which the article has been submitted; and agree to be accountable for all aspects of the work.

Funding

This work was supported by the National Natural Science Foundation of China (grant number: 91859107); Shanghai Science and Technology Committee (grant numbers: 18DZ1930102, 19411965500); Zhongshan Hospital, Fudan University (grant numbers: 2018ZSLC22, 2020ZSLC61); Shanghai Municipal Key Clinical Specialty (grant number: W2019-018); and Clinical Research Plan of SHDC (grant number: SHDC2020CR1029B).

Disclosure

The authors certify that they have no affiliations with, or involvement in, any organization or entity with any financial interest or non-financial interest in the subject matter or materials discussed in this manuscript.

References

1. Forner A, Reig M, Bruix J. Hepatocellular carcinoma. *Lancet*. 2018;391(10127):1301–1314. doi:10.1016/S0140-6736(18)30010-2
2. Vogel A, Cervantes A, Chau I, et al. Hepatocellular carcinoma: ESMO clinical practice guidelines for diagnosis, treatment and follow-up. *Ann Oncol*. 2018;29(Suppl 4):iv238–iv255. doi:10.1093/annonc/mdy308
3. Wang MD, Li C, Liang L, et al. Early and late recurrence of hepatitis B virus-associated hepatocellular carcinoma. *Oncologist*. 2020;25(10):e1541–e1551. doi:10.1634/theoncologist.2019-0944
4. Tung-Ping Poon R, Fan ST, Wong J. Risk factors, prevention, and management of postoperative recurrence after resection of hepatocellular carcinoma. *Ann Surg*. 2000;232(1):10–24. doi:10.1097/00000658-200007000-00003
5. An C, Kim DW, Park YN, Chung YE, Rhee H, Kim MJ. Single hepatocellular carcinoma: preoperative MR imaging to predict early recurrence after curative resection. *Radiology*. 2015;276(2):433–443. doi:10.1148/radiol.15142394
6. European Association for the Study of the Liver. EASL clinical practice guidelines: management of hepatocellular carcinoma. *J Hepatol*. 2018;69(1):182–236.
7. Kitao A, Matsui O, Yoneda N, et al. Gadoxetic acid-enhanced MR imaging for hepatocellular carcinoma: molecular and genetic background. *Eur Radiol*. 2020;30(6):3438–3447. doi:10.1007/s00330-020-06687-y
8. Liu X, Jiang H, Chen J, Zhou Y, Huang Z, Song B. Gadoxetic acid disodium-enhanced magnetic resonance imaging outperformed multidetector computed tomography in diagnosing small hepatocellular carcinoma: a meta-analysis. *Liver Transpl*. 2017;23(12):1505–1518. doi:10.1002/lt.24867
9. Guo J, Seo Y, Ren S, et al. Diagnostic performance of contrast-enhanced multidetector computed tomography and gadoxetic acid disodium-enhanced magnetic resonance imaging in detecting hepatocellular carcinoma: direct comparison and a meta-analysis. *Abdom Radiol*. 2016;41(10):1960–1972. doi:10.1007/s00261-016-0807-7
10. Ye F, Liu J, Ouyang H. Gadolinium ethoxybenzyl diethylenetriamine pentaacetic acid (Gd-EOB-DTPA)-enhanced magnetic resonance imaging and multidetector-row computed tomography for the diagnosis of hepatocellular carcinoma: a systematic review and meta-analysis. *Medicine*. 2015;94(32):e1157. doi:10.1097/MD.0000000000001157
11. Imai Y, Katayama K, Hori M, et al. Prospective comparison of Gd-EOB-DTPA-enhanced MRI with dynamic CT for detecting recurrence of HCC after radiofrequency ablation. *Liver Cancer*. 2017;6(4):349–359. doi:10.1159/000481416
12. Kim HD, Lim YS, Han S, et al. Evaluation of early-stage hepatocellular carcinoma by magnetic resonance imaging with gadoxetic acid detects additional lesions and increases overall survival. *Gastroenterology*. 2015;148(7):1371–1382. doi:10.1053/j.gastro.2015.02.051
13. Lee YJ, Lee JM, Lee JS, et al. Hepatocellular carcinoma: diagnostic performance of multidetector CT and MR imaging-a systematic review and meta-analysis. *Radiology*. 2015;275(1):97–109. doi:10.1148/radiol.14140690
14. Wei J, Jiang H, Gu D, et al. Radiomics in liver diseases: current progress and future opportunities. *Liver Int*. 2020;40(9):2050–2063. doi:10.1111/liv.14555
15. Chong HH, Yang L, Sheng RF, et al. Multi-scale and multi-parametric radiomics of gadoxetate disodium–enhanced MRI predicts microvascular invasion and outcome in patients with solitary hepatocellular carcinoma ≤ 5 cm. *Eur Radiol*. 2021. doi:10.1007/s00330-020-07601-2
16. Lambin P, Leijenaar RTH, Deist TM, et al. Radiomics: the bridge between medical imaging and personalized medicine. *Nat Rev Clin Oncol*. 2017;14(12):749–762. doi:10.1038/nrclinonc.2017.141
17. Cong WM, Bu H, Chen J, et al. Practice guidelines for the pathological diagnosis of primary liver cancer: 2015 update. *World J Gastroenterol*. 2016;22(42):9279–9287. doi:10.3748/wjg.v22.i42.9279
18. Hu HT, Shen SL, Wang Z, et al. Peritumoral tissue on preoperative imaging reveals microvascular invasion in hepatocellular carcinoma: a systematic review and meta-analysis. *Abdom Radiol*. 2018;43(12):3324–3330. doi:10.1007/s00261-018-1646-5
19. Hu H, Zheng Q, Huang Y, et al. A non-smooth tumor margin on preoperative imaging assesses microvascular invasion of hepatocellular carcinoma: a systematic review and meta-analysis. *Sci Rep*. 2017;7(1):15375. doi:10.1038/s41598-017-15491-6
20. Zhang R, Xu L, Wen X, et al. A nomogram based on bi-regional radiomics features from multimodal magnetic resonance imaging for preoperative prediction of microvascular invasion in hepatocellular carcinoma. *Quant Imaging Med Surg*. 2019;9(9):1503–1515. doi:10.21037/qims.2019.09.07
21. Nebbia G, Zhang Q, Arefan D, Zhao X, Wu S. Pre-operative microvascular invasion prediction using multi-parametric liver MRI radiomics. *J Digit Imaging*. 2020;33(6):1376–1386. doi:10.1007/s10278-020-00353-x
22. Portolani N, Coniglio A, Ghidoni S, et al. Early and late recurrence after liver resection for hepatocellular carcinoma: prognostic and therapeutic implications. *Ann Surg*. 2006;243(2):229–235. doi:10.1097/01.sla.0000197706.21803.a1
23. Imamura H, Matsuyama Y, Tanaka E, et al. Risk factors contributing to early and late phase intrahepatic recurrence of hepatocellular carcinoma after hepatectomy. *J Hepatol*. 2003;38(2):200–207. doi:10.1016/S0168-8278(02)00360-4
24. Okada S, Shimada K, Yamamoto J, et al. Predictive factors for postoperative recurrence of hepatocellular carcinoma. *Gastroenterology*. 1994;106(6):1618–1624. doi:10.1016/0016-5085(94)90419-7
25. Song W, Yu X, Guo D, et al. MRI-based radiomics: associations with the recurrence-free survival of patients with hepatocellular carcinoma treated with conventional transcatheter arterial chemoembolization. *J Magn Reson Imaging*. 2020;52(2):461–473. doi:10.1002/jmri.26977
26. Shan QY, Hu HT, Feng ST, et al. CT-based peritumoral radiomics signatures to predict early recurrence in hepatocellular carcinoma after curative tumor resection or ablation. *Cancer Imaging*. 2019;19(1):11. doi:10.1186/s40644-019-0197-5
27. Zhang Z, Chen J, Jiang H, et al. Gadoxetic acid-enhanced MRI radiomics signature: prediction of clinical outcome in hepatocellular carcinoma after surgical resection. *Ann Transl Med*. 2020;8(14):870. doi:10.21037/atm-20-3041
28. Zhang L, Hu J, Hou J, Jiang X, Guo L, Tian L. Radiomics-based model using gadoxetic acid disodium-enhanced MR images: associations with recurrence-free survival of patients with hepatocellular carcinoma treated by surgical resection. *Abdom Radiol*. 2021. doi:10.1007/s00261-021-03034-7
29. Kim S, Shin J, Kim DY, Choi GH, Kim MJ, Choi JY. Radiomics on gadoxetic acid-enhanced magnetic resonance imaging for prediction of postoperative early and late recurrence of single hepatocellular carcinoma. *Clin Cancer Res*. 2019;25(13):3847–3855. doi:10.1158/1078-0432.CCR-18-2861
30. Lee S, Kim SH, Lee JE, Sinn DH, Park CK. Preoperative gadoxetic acid-enhanced MRI for predicting microvascular invasion in patients with single hepatocellular carcinoma. *J Hepatol*. 2017;67(3):526–534. doi:10.1016/j.jhep.2017.04.024
31. American College of Radiology. CT/MRI LI-RADS® v2018 core; 2018. Available from: https://www.acr.org/Clinical-Resources/Reporting-and-Data-Systems/LI-RADS/CT-MRI-LI-RADS-v2018. Accessed May 17, 2021.

32. Amin MB, Greene FL, Edge SB, et al. *AJCC Cancer Staging Manual*. 8th ed. New York: Springer International Publishing; 2017.
33. Chan AWH, Zhong J, Berhane S, et al. Development of pre and post-operative models to predict early recurrence of hepatocellular carcinoma after surgical resection. *J Hepatol*. 2018;69(6):1284–1293. doi:10.1016/j.jhep.2018.08.027
34. Wei Y, Huang Z, Tang H, et al. IVIM improves preoperative assessment of microvascular invasion in HCC. *Eur Radiol*. 2019;29(10):5403–5414. doi:10.1007/s00330-019-06088-w
35. Wang W, Gu D, Wei J, et al. A radiomics-based biomarker for cytokeratin 19 status of hepatocellular carcinoma with gadoxetic acid-enhanced MRI. *Eur Radiol*. 2020;30(5):3004–3014. doi:10.1007/s00330-019-06585-y
36. Ji GW, Zhu FP, Xu Q, et al. Machine-learning analysis of contrast-enhanced CT radiomics predicts recurrence of hepatocellular carcinoma after resection: a multi-institutional study. *EBioMedicine*. 2019;50:156–165. doi:10.1016/j.ebiom.2019.10.057
37. Kim J, Choi SJ, Lee SH, Lee HY, Park H. Predicting survival using pretreatment CT for patients with hepatocellular carcinoma treated with transarterial chemoembolization: comparison of models using radiomics. *AJR Am J Roentgenol*. 2018;211(5):1026–1034. doi:10.2214/AJR.18.19507
38. Wang XH, Long LH, Cui Y, et al. MRI-based radiomics model for preoperative prediction of 5-year survival in patients with hepatocellular carcinoma. *Br J Cancer*. 2020;122(7):978–985. doi:10.1038/s41416-019-0706-0
39. Gu D, Xie Y, Wei J, et al. MRI-based radiomics signature: a potential biomarker for identifying glypican 3-positive hepatocellular carcinoma. *J Magn Reson Imaging*. 2020;52:1679–1687.
40. Xu X, Zhang HL, Liu QP, et al. Radiomic analysis of contrast-enhanced CT predicts microvascular invasion and outcome in hepatocellular carcinoma. *J Hepatol*. 2019;70(6):1133–1144. doi:10.1016/j.jhep.2019.02.023
41. Chen ZH, Zhang XP, Wang H, et al. Effect of microvascular invasion on the postoperative long-term prognosis of solitary small HCC: a systematic review and meta-analysis. *HPB*. 2019;21(8):935–944. doi:10.1016/j.hpb.2019.02.003
42. Jiang YQ, Cao SE, Cao S, et al. Preoperative identification of microvascular invasion in hepatocellular carcinoma by XGBoost and deep learning. *J Cancer Res Clin Oncol*. 2021;147(3):821–833. doi:10.1007/s00432-020-03366-9
43. Feng ST, Jia Y, Liao B, et al. Preoperative prediction of microvascular invasion in hepatocellular cancer: a radiomics model using Gd-EOB-DTPA-enhanced MRI. *Eur Radiol*. 2019;29(9):4648–4659. doi:10.1007/s00330-018-5935-8
44. Yang L, Gu D, Wei J, et al. A radiomics nomogram for preoperative prediction of microvascular invasion in hepatocellular carcinoma. *Liver Cancer*. 2018:1–14. doi:10.1159/000487148
45. Zhang S, Xu G, Duan C, et al. Radiomics analysis of MR imaging with Gd-EOB-DTPA for preoperative prediction of microvascular invasion in hepatocellular carcinoma: investigation and comparison of different hepatobiliary phase delay times. *Biomed Res Int*. 2021;2021:6685723.
46. Zhang Z, Jiang H, Chen J, et al. Hepatocellular carcinoma: radiomics nomogram on gadoxetic acid-enhanced MR imaging for early postoperative recurrence prediction. *Cancer Imaging*. 2019;19(1):22. doi:10.1186/s40644-019-0209-5
47. Shindoh J, Kobayashi Y, Kawamura Y, et al. Microvascular invasion and a size cutoff value of 2 cm predict long-term oncological outcome in multiple hepatocellular carcinoma: reappraisal of the American joint committee on cancer staging system and validation using the surveillance, epidemiology, and end-results database. *Liver Cancer*. 2020;9(2):156–166. doi:10.1159/000504193
48. Hwang S, Lee YJ, Kim KH, et al. The impact of tumor size on long-term survival outcomes after resection of solitary hepatocellular carcinoma: single-institution experience with 2558 patients. *J Gastrointest Surg*. 2015;19(7):1281–1290. doi:10.1007/s11605-015-2849-5
49. Yang L, Gu D, Wei J, et al. A radiomics nomogram for preoperative prediction of microvascular invasion in hepatocellular carcinoma. *Liver Cancer*. 2019;8(5):373–386. doi:10.1159/000494099
50. Renzulli M, Brocchi S, Cucchetti A, et al. Can current preoperative imaging be used to detect microvascular invasion of hepatocellular carcinoma? *Radiology*. 2016;279(2):432–442. doi:10.1148/radiol.2015150998
51. Kusano H, Han J, Bulthuis M, et al. Microvascular invasion in hepatocellular carcinoma is defined by tumor characteristics and aberrant angiogenesis in peritumoral tissue. *Hepatology*. 2013;58(4):1214A.
52. Yildiz E, Gokce G, Kilicarslan H, Ayan S, Goze OF, Gultekin EY. Prognostic value of the expression of Ki-67, CD44 and vascular endothelial growth factor, and microvessel invasion, in renal cell carcinoma. *BJU Int*. 2004;93(7):1087–1093. doi:10.1111/j.1464-410X.2004.04786.x
53. Miltiadous O, Sia D, Hoshida Y, et al. Progenitor cell markers predict outcome of patients with hepatocellular carcinoma beyond Milan criteria undergoing liver transplantation. *J Hepatol*. 2015;63(6):1368–1377. doi:10.1016/j.jhep.2015.07.025
54. Li JD, Xu XF, Han J, et al. Preoperative prealbumin level as an independent predictor of long-term prognosis after liver resection for hepatocellular carcinoma: a multi-institutional study. *HPB*. 2019;21(2):157–166. doi:10.1016/j.hpb.2018.06.1803
55. Iwadou S, Nouso K, Kuwaki K, et al. Time-dependent analysis of predisposing factors for the recurrence of hepatocellular carcinoma. *Liver Int*. 2010;30(7):1027–1032. doi:10.1111/j.1478-3231.2010.02252.x
56. Maeda T, Shimada M, Harimoto N, et al. Prognosis of early hepatocellular carcinoma after hepatic resection. *Hepato-Gastroenterology*. 2008;55(85):1428–1432.
57. Wu SJ, Lin YX, Ye H, Xiong XZ, Li FY, Cheng NS. Prognostic value of alkaline phosphatase, gamma-glutamyl transpeptidase and lactate dehydrogenase in hepatocellular carcinoma patients treated with liver resection. *Int J Surg*. 2016;36(Pt A):143–151. doi:10.1016/j.ijsu.2016.10.033
58. He LL, Liu XL, Zhang S, et al. Independent risk factors for disease recurrence after surgery in patients with hepatitis B virus-related hepatocellular carcinoma ≤3 cm in diameter. *Gastroenterol Rep*. 2019;7(4):250–257. doi:10.1093/gastro/goz009
59. Song P, Inagaki Y, Wang Z, et al. High levels of gamma-glutamyl transferase and indocyanine green retention rate at 15 min as preoperative predictors of tumor recurrence in patients with hepatocellular carcinoma. *Medicine*. 2015;94(21):e810. doi:10.1097/MD.0000000000000810
60. Lim C, Mise Y, Sakamoto Y, et al. Above 5 cm, size does not matter anymore in patients with hepatocellular carcinoma. *World J Surg*. 2014;38(11):2910–2918. doi:10.1007/s00268-014-2704-y
61. Shi M, Zhang C, Feng K, et al. [Micrometastasis distribution in liver tissue surrounding hepatocellular carcinoma]. *Zhonghua Zhong Liu Za Zhi [Chin J Oncol]*. 2002;24(3):257–260.
62. Lei Z, Li J, Wu D, et al. Nomogram for preoperative estimation of microvascular invasion risk in hepatitis B virus-related hepatocellular carcinoma within the milan criteria. *JAMA Surg*. 2016;151(4):356–363. doi:10.1001/jamasurg.2015.4257
63. Choi JY, Lee JM, Sirlin CB. CT and MR imaging diagnosis and staging of hepatocellular carcinoma: part I. Development, growth, and spread: key pathologic and imaging aspects. *Radiology*. 2014;272(3):635–654. doi:10.1148/radiol.14132361

64. Renzulli M, Biselli M, Brocchi S, et al. New hallmark of hepatocellular carcinoma, early hepatocellular carcinoma and high-grade dysplastic nodules on Gd-EOB-DTPA MRI in patients with cirrhosis: a new diagnostic algorithm. *Gut*. 2018;67(9):1674–1682. doi:10.1136/gutjnl-2017-315384
65. Wang WT, Yang L, Yang ZX, et al. Assessment of microvascular invasion of hepatocellular carcinoma with diffusion kurtosis imaging. *Radiology*. 2018;286(2):571–580. doi:10.1148/radiol.2017170515
66. Lubner MG, Smith AD, Sandrasegaran K, Sahani DV, Pickhardt PJ. CT texture analysis: definitions, applications, biologic correlates, and challenges. *Radiographics*. 2017;37(5):1483–1503. doi:10.1148/rg.2017170056